Nanodots and microwires of ZrO_2 grown on $LaAlO_3$ by photo-assisted metal–organic chemical vapor deposition*

Feng Guo(郭峰), Xin-Sheng Wang(汪薪生), Shi-Wei Zhuang(庄仕伟), Guo-Xing Li(李国兴)†, Bao-Lin Zhang(张宝林)‡, and Pen-Chu Chou(周本初)

State Key Laboratory on Integrated Optoelectronics, College of Electronic Science and Engineering, Jilin University, Changchun 130012, *China*

(Received 4 August 2015; revised manuscript received 7 October 2015; published online 20 December 2015)

ZrO_2 nanodots are successfully prepared on $LaAlO_3$ (LAO) (100) substrates by photo-assisted metal-organic chemical vapor deposition (MOCVD). It is indicated that the sizes and densities of ZrO_2 nanodots are controllable by modulating the growth temperature, oxygen partial pressure, and growth time. Meanwhile, the microwires are observed on the surfaces of substrates. It is found that there is an obvious competitive relationship between the nanodots and the microwires. In a growth temperature range from 500 °C to 660 °C, the microwires turn longest and widest at 600 °C, but in contrast, the nanodots grow into the smallest diameter at 600 °C. This phenomenon could be illustrated by the energy barrier, decomposition rate of $Zr(tmhd)_4$, and mobility of atoms. In addition, growth time or oxygen partial pressure also affects the competitive relationship between the nanodots and the microwires. With increasing oxygen partial pressure from 451 Pa to 752 Pa, the microwires gradually grow larger while the nanodots become smaller. To further achieve the controllable growth, the coarsening effect of ZrO_2 is modified by varying the growth time, and the experimental results show that the coarsening effect of microwires is higher than that of nanodots by increasing the growth time to quickly minimize ZrO_2 energy density.

Keywords: ZrO_2, photo-assisted MOCVD, nanodots, microwires

PACS: 81.15.Gh, 81.15.Kk **DOI:** 10.1088/1674-1056/25/2/028103

1. Introduction

ZrO_2 with excellent physical and chemical properties is attracting extensive interest in many fields nowadays. Because of the high-refractive index of ZrO_2, ZrO_2/Epoxy nano-composites are considered to be used as LED encapsulations.[1] ZrO_2 nanostructures have already been used as artificial pinning centers (APCs) to strongly pin the quantized vortices in high temperature superconductors (HTS).[2] ZrO_2 is the only transition metal oxide which possesses not only acidic sites but also alkaline sites and can be used as both catalyst and catalyst carrier.[3–5] Especially, owing to the excellent chemical stability and larger relative surface area, catalytic performance of ZrO_2 nanostructure can be much better than bulk material.[6,7] Based on these charming applications, an investigation about the way to grow controllable nanostructures of ZrO_2 is essential.

Varieties of methods have been utilized for ZrO_2 fabrication, such as pulsed laser deposition (PLD),[8] atomic layer deposition (ALD),[9] and sputtering.[10] Compared with these methods, metal–organic chemical vapor deposition (MOCVD) technology is a proven fabrication technology and versatile process for high quality/large-area production of materials with high growth rates.[11–15] Various papers have reported the preparation of ZrO_2 films by MOCVD technology, and discussed the growth mechanism.[16,17] However, there are no reports on ZrO_2 nanostructures prepared by MOCVD.

Compared with the ordinary heat treatment technology, the photo-activation in the photo-assisted process possesses some advantages,[18,19] for example, superconducting $YBa_2Cu_3O_{7-\delta}$ (YBCO), $GdBa_2Cu_3O_{7-\delta}$ (GdBCO) films prepared by photo-assisted MOCVD have good alignments and high growth speeds.[20–22] Experimental results indicated that photo-assisted annealing had obviously a higher oxidization rate for the YBCO films in one oxygen atmosphere than thermal annealing.[23] In the present work, the photo-assisted MOCVD is applied to the preparation of ZrO_2 nanostructure for the first time.

Quite a lot of reports show that growth parameters have significant effects on the morphologies and physical properties of nanostructures prepared by MOCVD. For example, in a growth temperature range from 500 °C to 610 °C, the island density of GaSb first increases and then decreases.[24] Furthermore, there is a linear relationship between the size of ZnO nanodots and the growth time.[25] Oxygen partial pressure is also an important factor in the growth of Y_2O_3 by MOCVD.[26] So the effect of growth parameters on the surface morphologies of ZrO_2 is worthy of investigation. Our study shows that the morphologies of ZrO_2 could be controlled through systematically modulating the growth parameters, such as growth temperature, oxygen partial pressure and

*Project supported by the National Natural Science Foundation of China (Grant No. 51002063) and the International Science and Technology Cooperation Program of Science and Technology Bureau of Changchun City, China (Grant No. 12ZX68).

†Corresponding author. E-mail: liguoxing@jlu.edu.cn

‡Corresponding author. E-mail: zbl@jlu.edu.cn

© 2016 Chinese Physical Society and IOP Publishing Ltd

growth time. The effects of the growth parameters on the surface morphologies of ZrO_2 are systematically analyzed and the growth mechanism is discussed.

2. Experiments

Hetero-epitaxial ZrO_2 was grown on a single crystal LAO (100) substrate with a perovskite pseudocubic structure by a photo-assisted MOCVD system. The structure of the photo-assisted MOCVD system has been reported in our previous work.[21] Solid metal–organic source of $Zr(tmhd)_4$ (tmhd = 2, 2, 6, 6-tetramethyl-3, 5-heptanedionate) was used as a precursor of Zr. A mixture containing oxygen and nitrous oxide with a volume ratio of 3:2 was used as an oxidizing agent.[27] $Zr(tmhd)_4$ was sublimated at 230 °C in a carrier gas of high purity (99.999%) argon with a molar flow rate at 2×10^{-4} mol/min to participate in the reaction. The total pressure in the reaction chamber was controlled and set at 1000 Pa. Oxygen partial pressure was determined by the flow rate of the oxidizing gas, with the flow rate of argon kept constant.

For these experiments the dependence of the morphologies of ZrO_2 on the growth parameters was investigated. Those growth parameters including growth temperature, oxygen partial pressure, and growth time were set and controlled according to a set of primary experiments. Firstly, the growth temperature was varied from 500 °C to 660 °C, while the oxygen partial pressure and growth time were set at 752 Pa and 60 s, respectively. Secondly, ZrO_2 nanostructures were fabricated at various oxygen partial pressures ranging from 451 Pa to 752 Pa. The growth temperature was kept constant (at 600 °C), and the growth time was set to 60 s. Finally, the growth times were set to 20 s, 40 s, and 60 s while the oxygen partial pressure was set to 752 Pa at the growth temperature of 600 °C.

Surface morphologies of ZrO_2 were investigated by an atomic force microscope (AFM; iCON, Veeco) with the tapping mode at room temperature. Statistical analyses of AFM images including the diameter, height, and density of nanodots as well as the length, width, and height of microwires were carried out by NanoScope Analysis software.

3. Results and discussion

3.1. Dependence of nanodots on growth parameters

The effect of growth temperature on the surface morphologies of ZrO_2 nanostructures is determined at constant oxygen partial pressure (752 Pa) and growth time (60 s) as shown in Fig. 1. It is clearly seen that the morphologies of ZrO_2 nanostructures are strongly influenced by the growth temperature and most of the nanodots present a typical isotropic dome-like morphology. It is found that as the temperature increases from 500 °C to 600 °C, the nanodots change from large and sparse islands to smaller and more closely packed ones. However, when the temperature increases to 660 °C, the sizes of nanodots gradually become larger while their density becomes lower.

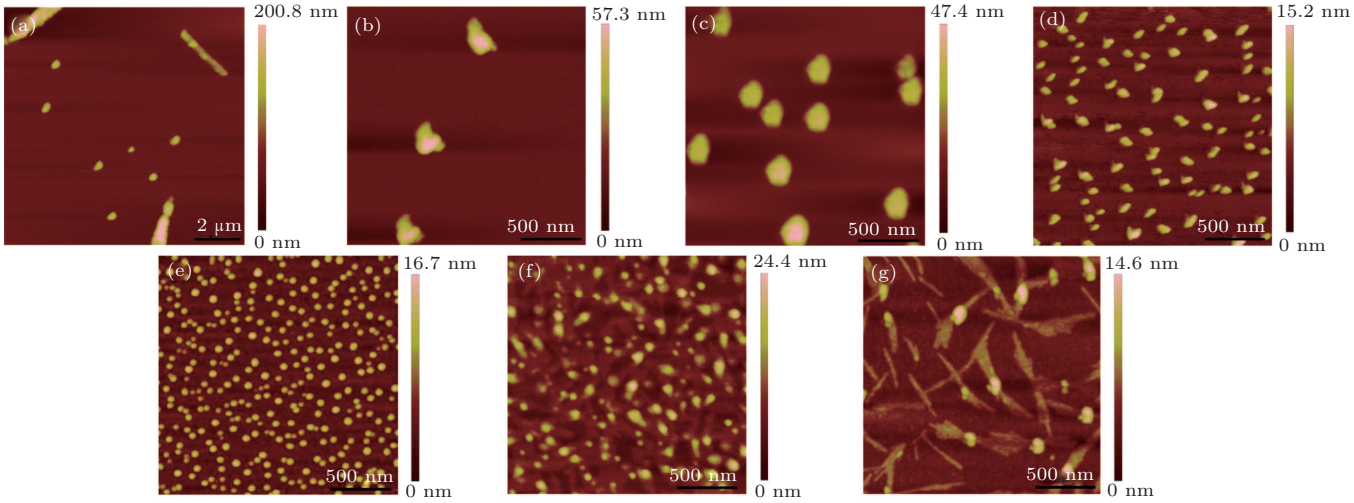


Fig. 1. (color online) The 2 μm × 2 μm two-dimensional AFM images of the ZrO_2 nanodots on LAO (100) at various substrate temperatures: (a) 500 °C (scaled: 10 μm × 10 μm), (b) 525 °C, (c) 550 °C, (d) 575 °C, (e) 600 °C, (f) 630 °C, and (g) 660 °C.

Figure 2 shows the sizes and densities of ZrO_2 nanodots each as a function of growth temperature. As shown in Fig. 2(a), the diameter and height of nanodots first decrease and then increase with growth temperature increasing from 500 °C to 660 °C. At 500 °C, the average height of nanodots is 94 nm, and the average diameter is 401.1 nm. The average height of nanodots reaches a minimum value of 7.7 nm at 575 °C while the minimum average diameter is 81.1 nm at 600 °C in the range of 500 °C–600 °C. As temperature increases to 660 °C, the average height and diameter of nanodots are up to 11.5 nm and 152.8 nm, respectively. However, the trend of nanodot density is quite different. When the

growth temperatures are 500 °C and 660 °C, the densities of nanodots are only 7.0×10^6 cm^{-2} and 3.3×10^8 cm^{-2}, respectively. The maximum value of the density is 7.4×10^9 cm^{-2} at 600 °C (Fig. 2(b)). Moreover, there are two different temperature regions, in which the influences of growth temperature on the density and average size are different. A low density and large diameter are obtained at a lower temperature. This could be explained by the low decomposition rate of $Zr(tmhd)_4$ at the low temperature, leading to less nucleation sites, and the low migration rate resulting in a short surface mobility distance. This similar behavior was also reported in Ref. [28]. As the surface migration rate increases with temperature, the nanodots become small and closely packed. When the temperature is further increased, a high surface migration rate could result in a significant coarsening.

The controllable growth of ZrO_2 nanodots is difficult to achieve by an isolated set of experiments. For investigating the kinetic processes involved in the growth of ZrO_2 nanodots on LAO (100) substrates, a series of samples is prepared at oxygen partial pressures from 451 Pa to 752 Pa at fixed growth temperature (600 °C) and growth time (60 s) as shown in Fig. 3. The results show that the oxygen partial pressure has a great influence on the sizes and densities of ZrO_2 nanodots. As observed from Fig. 3, when oxygen partial pressure increases from 451 Pa to 752 Pa, the nanodots become small and dense in terms of the growth trend of nanodots. The variations of ZrO_2 nanodot size and density are shown in Fig. 4. In Fig. 4, when the oxygen partial pressure changes from 451 Pa to 752 Pa, the average diameter and height of ZrO_2 nanodots decrease from 128.8 nm to 81.1 nm, and from 18.1 nm to 10 nm, respectively, while the density increases from 7.3×10^8 cm^{-2} to 7.4×10^9 cm^{-2}. The total pressure and the amount of $Zr(tmhd)_4$ provided for the reactor chamber are fixed. Variation of oxygen partial pressure is replaced by the same amount of argon partial pressure. Different oxygen partial pressure can affect the efficiency of the source in the reaction, leading to changes in the size and density of nanostructures. We assume that at high partial pressure of oxygen, a sufficient amount of oxidizing gas could make more Zr atoms involved in the reaction, so nucleation would be rapid and massive on the substrate surface. This could be a reason why the nanodots are relatively small and dense at an oxygen partial pressure of 752 Pa.

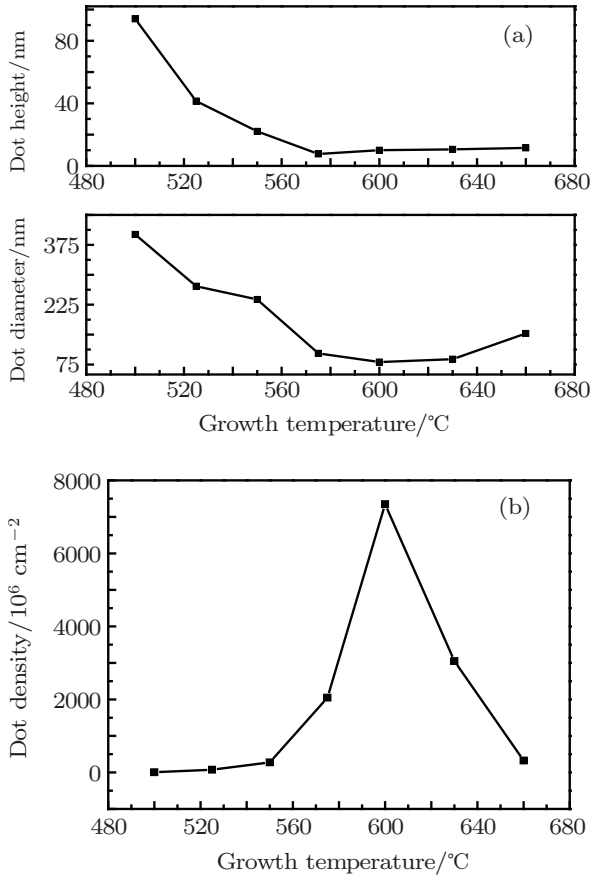


Fig. 2. (a) Average height and diameter of ZrO_2 nanodots, and (b) density of nanodots versus growth temperature.

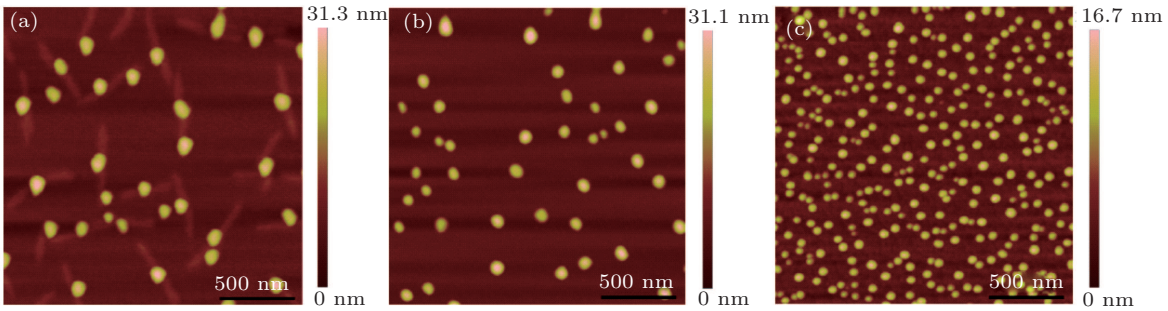


Fig. 3. (color online) The 2 μm × 2 μm two-dimensional AFM images of ZrO_2 nanodots on LAO (100) at different oxygen partial pressures: (a) 451 Pa, (b) 602 Pa, (c) 752 Pa.

For further discussing the mechanism of the growth process of nanodots, the growth time is modulated at a fixed temperature of 600 °C and oxygen partial pressure of 752 Pa, the effect of growth time on the ZrO_2 nanostructures is as follows (Fig. 5). The ZrO_2 nanostructures each have an isotropic dome-like shape. The dependences of the average size and density of ZrO_2 nanodots on growth time are shown in Fig. 6. As shown in this figure, the diameter of ZrO_2 nanodot be-

comes larger with the increase of growth time, while the height is constant. The average diameter and height of nanodots are 61.5 nm and 10.4 nm, respectively, when the growth time is 20 s. With the growth time increasing up to 60 s, the average diameter reaches 82.6 nm, while the average height is only 10.1 nm. This indicates that the ZrO_2 nanodots tend to laterally grow rather than vertically grow. Meanwhile, the density of nanodots is about twice as large as the initial density.

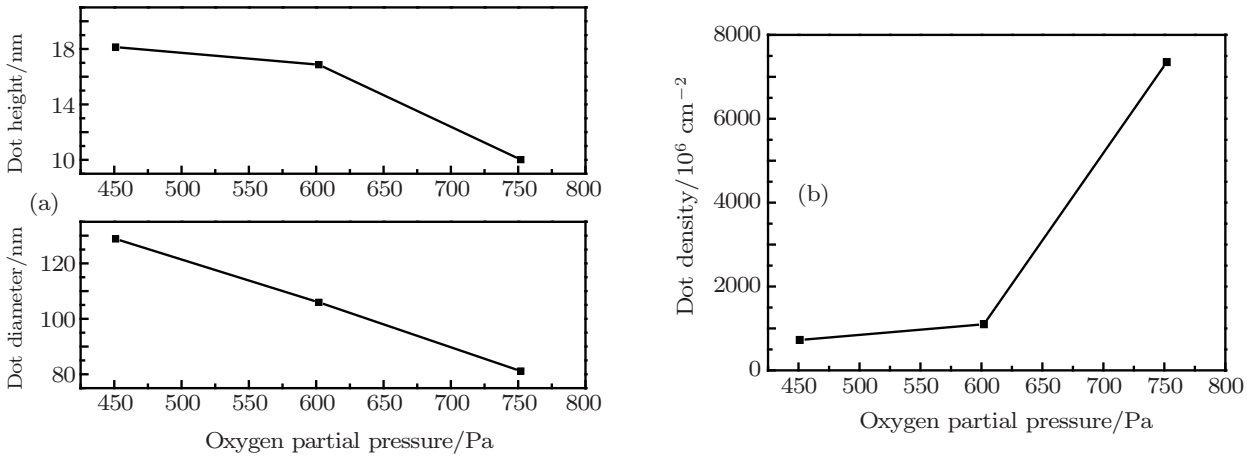


Fig. 4. (a) Average height and diameter of ZrO_2 nanodots, and (b) density versus oxygen partial pressure.

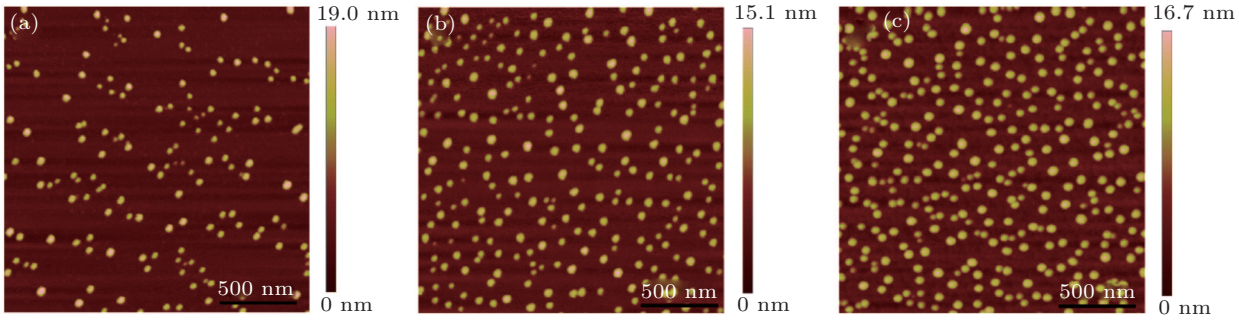


Fig. 5. (color online) The 2 μm × 2 μm two-dimensional AFM images of ZrO_2 nanostructures on LAO (100) at various growth times: (a) 20 s, (b) 40 s, (c) 60 s.

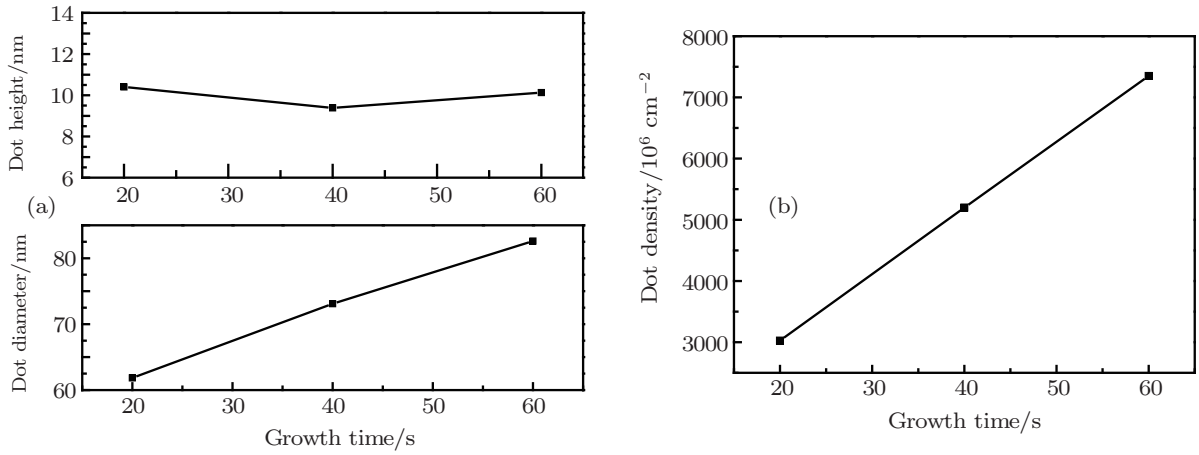


Fig. 6. Growth time dependences of (a) average size and (b) density of ZrO_2 nanodots on LAO (100) substrates grown by photo-assisted MOCVD.

3.2. Dependence of microwires on growth parameters

Surprisingly, the anisotropic ZrO_2 microwires are found on LAO (100) substrates. These mutually perpendicular microwires constitute a network structure. Owing to the large sizes of microwires compared with those of the nanodots, the nanodots cannot be seen. It is found that growth conditions also have a great influence on the morphologies of microwires. Besides, experimental results indicate that the two different ZrO_2 morphologies are in competition.

The surface morphologies of ZrO_2 microwires grown at various growth temperatures are shown in Fig. 7. The scanned area for each AFM image is 50 μm × 50 μm. The size of microwire increases with the temperature increasing from 500 °C to 600 °C, but when the temperature is varied from 600 °C to 660 °C, the size begins to decline. The length and width of the microwire reach maxima of 17.23 μm and 2.77 μm at 600 °C, respectively. However, the height reaches a maximum of 471.3 nm at 630 °C. Figure 8 shows that the competitive relationship between the diameter of nanodots and the length of microwires can be seen clearly. From 500 °C to 600 °C, the growth of microwires dominates gradually, which is mainly due to the fact that the energy barrier of the microwire is lower at high temperature, which is similar to the growth of CGO on the LAO.[29] When the temperature is higher than 600 °C, the diameter of nanodots slightly increases. At 660 °C, the layered structure is found under the nanodots (as seen in Fig. 1(g)), while the size of microwires drops rapidly. This is related to the higher mobility of atoms and the higher volatility of the reaction atoms at high temperature.

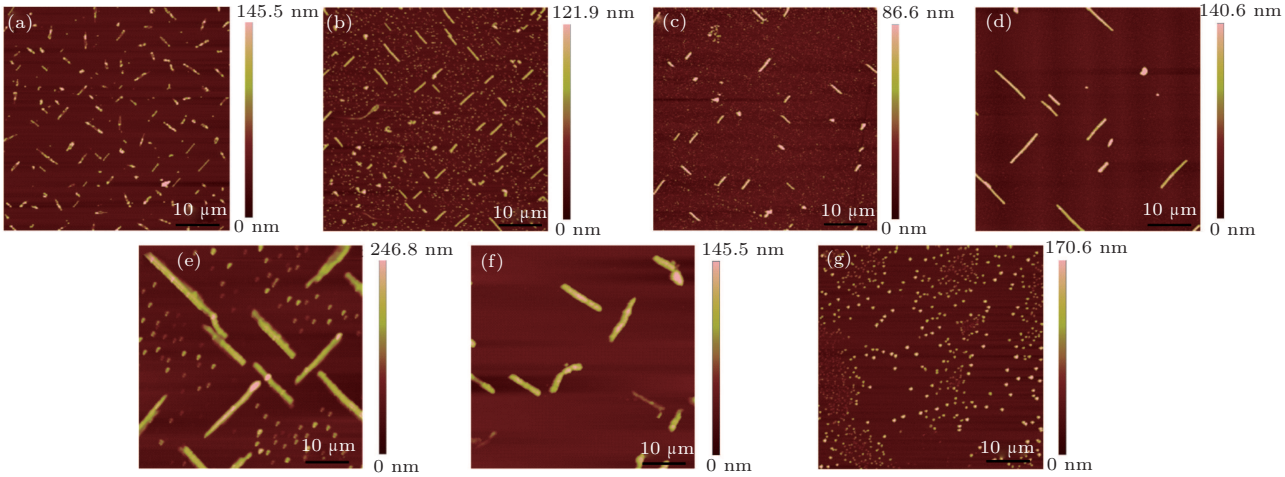


Fig. 7. (color online) The 50 μm × 50 μm two-dimensional AFM images of ZrO_2 microwires on LAO (100) at various growth temperatures: (a) 500 °C, (b) 525 °C, (c) 550 °C, (d) 575 °C, (e) 600 °C, (f) 630 °C, and (g) 660 °C.

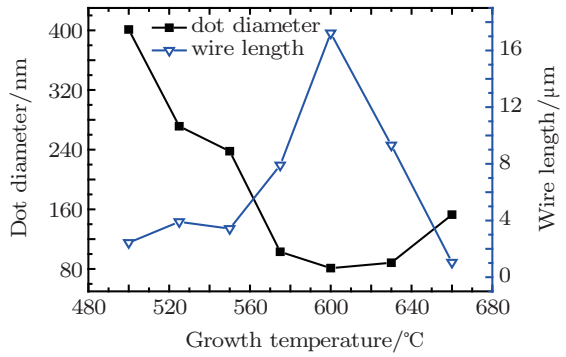


Fig. 8. (color online) Diameter of nanodots and length of microwires versus growth temperature, showing their competitive relationship.

In order to further understand the competitive relationship between the ZrO_2 nanodot and microwire, the microwires are prepared at various oxygen partial pressures, with growth temperature (600 °C) and time (60 s) kept unchanged. Figure 9 shows AFM images of the morphologies of ZrO_2 microwires on LAO substrates at different oxygen partial pressures. As shown in Fig. 9, the height, width, and length of microwires all increase with oxygen partial pressure increasing. For an oxygen partial pressure of 752 Pa, the width and length of the microwire are 2.77 μm and 17.23 μm, respectively, while the width and length of microwires are only about half those when the oxygen pressure drops to 451 Pa, and the height of the microwire also decreases from 152.2 nm to 127.5 nm. While the variation trend of the nanodots is different, the competitive relationship between the diameter of nanodots and the length of microwires versus oxygen pressure can be seen in Fig. 10.

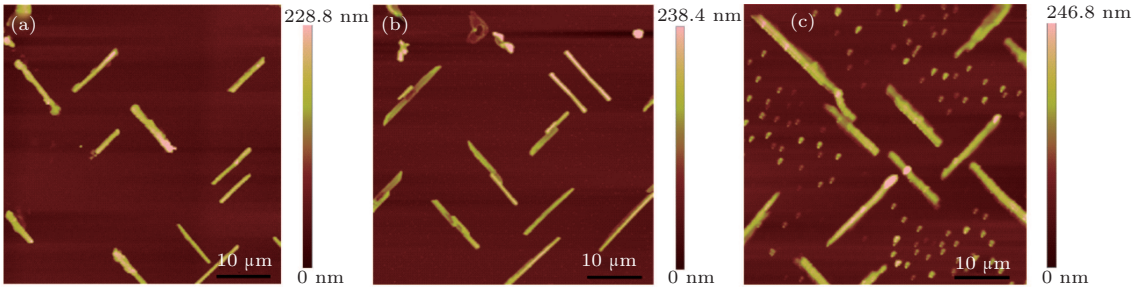


Fig. 9. (color online) The 50 μm × 50 μm two-dimensional AFM images of ZrO_2 microwires on LAO (100) at different oxygen partial pressures: (a) 451 Pa, (b) 602 Pa, (c) 752 Pa.

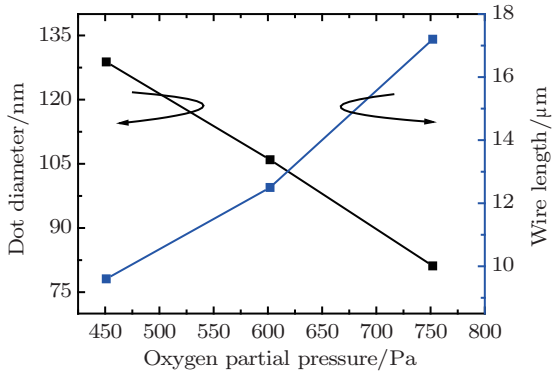


Fig. 10. (color online) Variations of diameter of nanodots and the length of microwires with oxygen partial pressure, showing their competitive relationship.

In addition, the influence of growth time on the competition between the nanodots and the microwires is also investigated. As mentioned above, the ZrO_2 nanodots tend to laterally grow rather than vertically grow. As for the ZrO_2 microwires, a similar law is found in Fig. 11. The AFM images show the morphologies of ZrO_2 microwires for different growth times. With the increasing of growth time, the ZrO_2 microwires continuously coarsen. However, the coarse efficiencies of anisotropic ZrO_2 microwires in different directions are different. Compared to the microwire width of 1.24 μm at 20 s, the width of microwires is raised to 2.33 times at 60 s, while the length of the ZrO_2 microwire is increased from 5.12 μm to 17.23 μm. It is similar to the growth trend of nanodots, the height of microwires is changed slightly. When the growth time is 20 s, the height of microwires is 133.7 nm. However, as the time increases up to 60 s, the increment of height is only 18.5 nm. This shows that the anisotropy ZrO_2 microwires are more inclined to coarsen in the long axis direction. Figure 12 shows the average diameter of nanodots and the average length of microwires each as a function of growth time, it can be found that the competitive relationship also exists. The diameter of nanodots is increased to 1.34 times of the original diameter, while the length of ZrO_2 microwire increases to 3.37 times. So ZrO_2 is more inclined to strengthen the length of ZrO_2 microwire than the growth of nanodot grown at 600 °C and the oxygen partial pressure of 752 Pa. According to the experimental results of Marta Gibert *et al.*,[30] we infer that it is because of this phenomenon that ZrO_2 energy density can be quickly minimized.

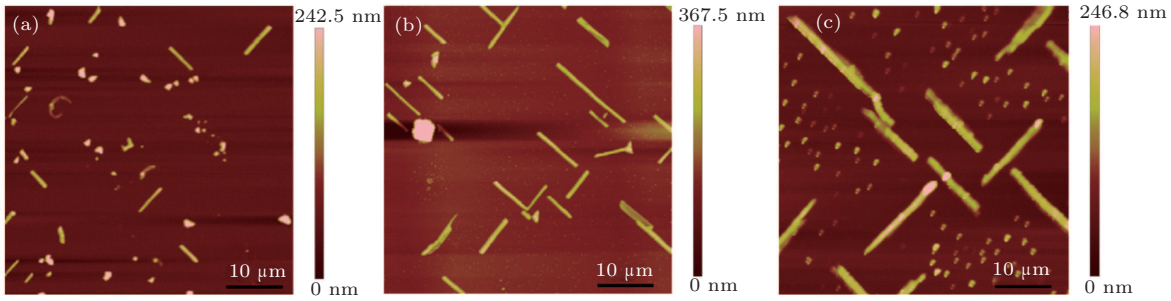


Fig. 11. (color online) The 50 μm × 50 μm two-dimensional AFM images of ZrO_2 microwires on LAO (100) at various growth times: (a) 20 s, (b) 40 s, (c) 60 s.

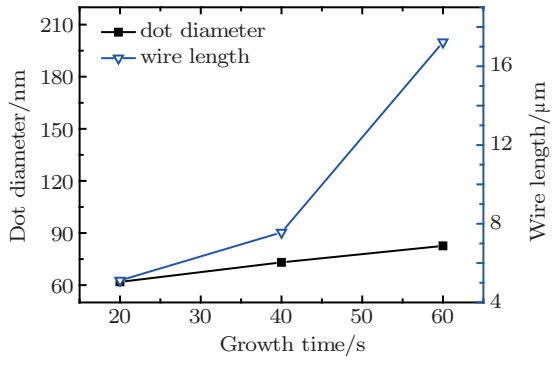


Fig. 12. (color online) Variations of diameter of nanodots and length of microwires with growth time, showing their competitive relationship.

4. Conclusions

In this work, the growth of ZrO_2 nanostructures on $LaAlO_3$ (LAO) (100) substrates by the photo-assisted MOCVD is investigated, and two kinds of completely different surface morphologies of ZrO_2 are observed, i.e., ZrO_2 nanodots and microwires. The experimental results show that the two kinds of surface morphologies of ZrO_2 depend strongly on the growth parameters. At high oxygen partial pressure, the growth of microwires tends to be dominant. With increasing the growth time, the microwires of ZrO_2 preferentially coarsen to minimize ZrO_2 energy density. Similarly, there is a clear competitive relationship between the ZrO_2 nanodot and microwire in the process of modulating the growth temperature. When grown at low temperature, the nanodot presents the shape of large and sparse ones because of the less nucleation sites and the low migration rate of atoms. With increasing the growth temperature, the nanodots become small and dense. When the temperature increases further, a high surface migration rate could result in a significant coarsening. The morphologies of nanodots are characterized by large and sparse ones again. However, the trend of microwires is totally different. Compared with the size at 600 °C, the size of mi-

crowires is small at 500 °C, and so is it at 660 °C. Our experimental results demonstrate the feasibility for the controllable growth of ZrO_2 by photo-assisted MOCVD.

References

[1] Tao P, Li Y, Richard S and Linda S 2013 *J. Appl. Polym. Sci.* **130** 3785
[2] Moutalbi N, Ouerghi A, Djurado E, Noudem J G and M'chirgui A 2011 *Physica C* **471** 97
[3] Wang Y, Nie X A and Liu Z X 2015 *J. Am. Oil Chem. Soc.* **92** 813
[4] Damyanovaa S, Centenob M A, Petrova L and Grangec P 2001 *Spectrochim. Acta* **57** 2495
[5] Nozawa T, Sato S and Takahashi R 2009 *Top. Catal.* **52** 609
[6] Behbahani F K, Ziaei P, Fakhroueian Z and Doragi N 2011 *Monatsh. Chem.* **142** 901
[7] Li Y, Wang Y H and Xu B Q 2005 *Chem. J. Chin. Univ.* **26** 1325
[8] Zhang W, Cui Y, Hu Z G, Yu W L, Sun J, Xu N, Ying Z F and Wu J D 2012 *Thin Solid Films* **520** 6361
[9] Kim Y, Koo J, Han J W, Choi S, Jeon H and Park C G 2002 *J. Appl. Phys.* **92** 5443
[10] Venkataraj S, Kappertz O, Weis H, Drese R, Jayavel R and Wuttig M 2002 *J. Appl. Phys.* **92** 3599
[11] Kong X T, Zhou X L, Li S Y, Qiao L J, Liu H G, Wang W and Pan J Q 2015 *Chin. Phys. Lett.* **32** 037301
[12] Ni Y Q, He Z Y, Zhong J, Yao Y, Yang F, Xiang P, Zhang B J and Liu Y 2013 *Chin. Phys. B* **22** 088104
[13] Feng X J, Zhao C S, Li Z, Luo Y and Ma J 2015 *Mater. Res. Bull.* **70** 354
[14] Yang X L, Zhang G Y, Fan G H and Xing H Y 2010 *Acta Phys. Sin.* **59** 504 (in Chinese)
[15] Sun P, Li J J, Deng J, Han J, Ma L Y and Liu T 2013 *Acta Phys. Sin.* **62** 026801 (in Chinese)
[16] Dang V S, Banerjee M, Zhu H Z, Srinivasan N B, Parala H, Pfetzing-Micklich J, Wieck A D and Devi A 2014 *Chem. Vap. Deposition* **20** 320
[17] Chen Z, Prud'homme N, Wang B and Ji V 2011 *Surf. Coat. Tech.* **206** 405
[18] Li X P, Zhang B L, Zhu H C, Dong X, Xia X C, Cui Y G, Huang K K and Du G T 2008 *Appl. Surf. Sci.* **254** 2081
[19] Singh R, Sinha S, Thakur R P S and Chou P C 1991 *Appl. Phys. Lett.* **58** 1217
[20] Fang X J, Li G X, Li S W, Zhao L, Li W C, Zhang B L, Du G T, Chou P C, Li H, Zuo R, He L and Chen C P 2008 *Physica C* **468** 1053
[21] Li G X, Fang X J, Zhao L, Li S W, Gao Z M, Li W C, Yin J Z, Zhang B L, Du G T, Chou P C, He L and Chen C P 2008 *Physica C* **468** 2213
[22] Li W, Li S W, Li G X, Zhang B L and Chou P C 2013 *IEEE Trans. Appl. Supercond.* **23** 7200606
[23] Li G X, Li S W, Li W, Wang X S, Guo F, Zhang B L and Chou P C 2014 *Physica C* **507** 17
[24] Wang L K, Liu R J, Yang H Y, Lü Y, Li G X, Zhang Y T and Zhang B L 2014 *Chin. Phys. B* **23** 088110
[25] Zhang J X, Cui X J, Shi Z F, Wu B, Zhang Y T and Zhang B L 2014 *Superlattices Microstruct.* **71** 23
[26] Li W, Li S W, Li G X, Zhang B L and Chou P C 2013 *Appl. Surf. Sci.* **264** 748
[27] Chou P C, Zhong Q, Li Q L, Abazajian K, Ignatiev A, Wang C Y, Deal E E and Chen J G 1995 *Physica C* **254** 93
[28] Yang H Y, Liu R J, Lü Y, Wang L K, Li T T, Li G X, Zhang Y T and Zhang B L 2014 *Chem. Res. Chin. Univ.* **30** 13
[29] Gibert M, Abellan P, Martínez L, Roman E, Crespi A, Sandiumenge F, Puig T and Obradors X 2011 *CrystEngComm* **13** 6719
[30] Gibert M, García A, Puig T and Obradors X 2010 *Phys. Rev. B* **82** 165415